

# EVDodge: Embodied AI For High-Speed Dodging On A Quadrotor Using Event Cameras

Nitin J. Sanket<sup>1</sup>, Chethan M. Parameshwara<sup>1</sup>, Chahat Deep Singh<sup>1</sup>, Ashwin V. Kuruttukulam<sup>1</sup>,  
Cornelia Fermüller<sup>1</sup>, Davide Scaramuzza<sup>2</sup>, Yiannis Aloimonos<sup>1</sup>

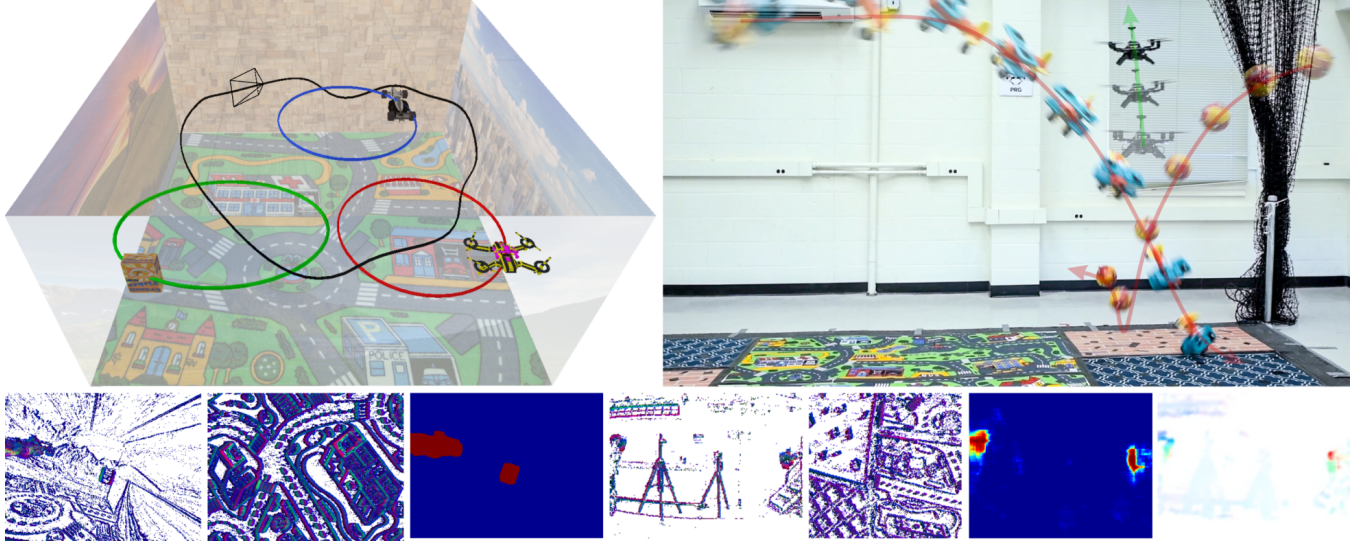


Fig. 1. Top row (left to right): Simulation environment used to generate event frames to train our networks, real quadrotor running the network trained on simulation dodging two obstacles thrown simultaneously at it. Bottom row (left to right): Front and down facing event frame generated from simulation, simulation ground truth segmentation corresponding to front facing event frame, front and down facing event frame in real experiment, predicted segmentation mask corresponding to real front facing event frame and finally, segmentation flow output which includes both segmentation and optical flow. *All the images in this paper are best viewed in color.*

**Abstract**—The human fascination to understand ultra-efficient agile flying beings like birds and bees have propelled decades of research on trying to solve the problem of obstacle avoidance on micro aerial robots. However, most of the prior research has focused on static obstacle avoidance. This is due to the lack of high-speed visual sensors and scalable visual algorithms. The last decade has seen an exponential growth of neuromorphic sensors which are inspired by nature and have the potential to be the de facto standard for visual motion estimation problems.

After re-imagining the navigation stack of a micro air vehicle as a series of hierarchical competences, we develop a purposive artificial intelligence based formulation for the problem of general navigation. We call this AI framework “Embodied AI” - AI design based on the knowledge of agent’s hardware limitations and timing/computation constraints. Following this design philosophy we develop a complete AI navigation stack for dodging multiple dynamic obstacles on a quadrotor with a monocular event camera and computation. We also present an approach to directly transfer the shallow neural networks trained in simulation to the real world by subsuming pre-processing using a neural network into the pipeline.

Nitin J. Sanket and Chethan M. Parameshwara contributed equally to this work. (Corresponding author: Nitin J. Sanket.)

<sup>1</sup>Perception and Robotics Group, University of Maryland Institute for Advanced Computer Studies, University of Maryland, College Park.

<sup>2</sup>Robotics and Perception Group, Dep. of Informatics, University of Zurich, and Dep. of Neuroinformatics, University of Zurich and ETH Zurich.

We successfully evaluate and demonstrate the proposed approach in many real-world experiments with obstacles of different shapes and sizes, achieving an overall success rate of 70% including objects of unknown shape and a low light testing scenario. To our knowledge, this is the first deep learning based solution to the problem of dynamic obstacle avoidance using event cameras on a quadrotor. Finally, we also extend our work to the pursuit task by merely reversing the control policy proving that our navigation stack can cater to different scenarios.

**Keywords** – Embodied AI, Artificial Intelligence, Quadrotor, Visual-Based Navigation, Aerial Systems: Perception and Autonomy, Deep Learning in Robotics and Automation, Collision Avoidance, Event camera.

## SUPPLEMENTARY MATERIAL

The accompanying video and supplementary material are available at [prg.cs.umd.edu/EVDodge](http://prg.cs.umd.edu/EVDodge). The accompanying code and dataset will be released on the same link after the acceptance for publication.

## I. INTRODUCTION AND PHILOSOPHY

The never-ending quest to understand and mimic ultra-efficient flying agents like bees, flies, and birds have fueled the human fascination to create autonomous, agile and ultra-efficient flying robots. These small aerial robots are not only utilitarian but are much safer to operate in static or

dynamic environments and around other agents as compared to their larger counterparts. Simply using “off-the-shelf” computer vision algorithms finds little use on these small aerial robots due to their limited computing power and tight time bounds which escalate with a decrease in size. Hence, recently a new philosophy of algorithmic design for small aerial robots was presented in [1] based on the conceptualization of a flying agent as a set of hierarchical competences. The heart of these competencies is fueled by the pioneering work on active vision [2].

Building on the formalism presented in [1], we present an Artificial Intelligence (AI) formulation based on deep learning for the problem of general navigation of a small flying agent in this paper. To prove the practicality of the approach, we apply this formulation to the problem of evading/dodging/avoiding dynamic obstacles in the scene with a monocular camera. This AI framework is different from standard approaches as it is purposive – to make the flying efficient in terms of computation and speed whilst being able to reuse competences to solve higher order tasks. We call this formulation *Embodied AI* – AI design based on the knowledge of the agent’s hardware limitations and timing/computation constraints.

Our system has a front facing monocular event based camera, a lower resolution downfacing event based monocular camera coupled with sonar and an IMU. Event-based cameras are chosen because of their high temporal resolution, low-latency, high dynamic range and data sparsity (capturing well-moving contours which is tailor-made for navigation).

#### A. Independent Motion Detection and Ego-motion/Odometry: Two sides of the same coin

The first step in evasion/dodging is to find the Independently Moving Objects (IMOs) whilst also estimating self-movement. However, IMO detection is one of the more complex problems in the field of visual navigation. One might intuit that without knowing one’s own motion it is impossible to estimate others’ movements, indeed this is true. This fact compelled the pioneers in the field of visual navigation to extensively work on egomotion/odometry. Ever since, the concept of “vection” [3] was introduced, it has taken on many faces with its most decorated being the usage of optical flow to recover odometry. Recently, information from complementary sensors such as Inertial Measurement Units (IMUs) has given rise to the field of Visual Inertial Odometry [4] [5]. Other works try to add semantic information to enhance the quality of odometry which makes up for the lack of sensors by adding strong priors about the scene [6] [7]. Most works in the literature focus on egomotion estimation in static scenes which are seldom encountered in the real world. To account for moving objects, these algorithms implement a set of outlier rejection schemes to detect IMOs. We would like to point out that by carefully concocting these “outliers” one can estimate both egomotion and IMO motion. Thus, ego-motion and IMO motion are chicken-egg problems: you need the solution

of one to solve the other. This paves the path for joint optimization of egomotion and IMO motion.

#### B. Image stabilization as a key to independent motion segmentation

Keen readers might have contrived that by performing the process of image stabilization IMOs would “stand-out”. Indeed, this was the approach most robust algorithms used in the last two decades. A similar concept was adapted in some recent works on event-based cameras for detecting IMOs [8], [9]. However, for a flying visual agent, merely detecting an IMO is not enough, it should be able to estimate the IMO’s 3D motion to take appropriate actions like dodge or intercept/pursuit.

In this paper, we propose a novel approach for detecting IMO’s from event image sequences and reasoning about their 3D motions in order to perform the task of dodging and then later extend it to the task of pursuit. Also, we introduce a new perspective of solving problems of this kind (visual geometric problems) using deep learning in simulation.

#### C. Learning IMO’s location and motion using simulation for generalization onto real scenes

Formulating the problem such that the building blocks can be re-purposed is inspired by the central conception of Embodied AI. Such a formulation lends itself to be forged by a network of shallow networks. As each of the networks is performing a modest task, each network can be realized using a shallow network without significant loss of performance. Such a formulation has the palpable advantage of “not overfitting” to the dataset during training due to the dearth of a number of learnable parameters. In this paper, we present a way to obtain “unlimited amount of training data” by synthetically generating them in various scenes. Having the masks for the location of the IMOs, we learn how to produce the optical flow in those IMO regions. It turns out, that because the gist of our problem has to do with boundaries in motion, the learning generalizes very well to real scenes. This is especially true for the event-based sensor employed in this paper.

The key contributions of this paper are given below (Fig. 1):

- Conception and realization of self and IMO motion estimation on a quadrotor using a network of shallow networks.
- Propose the concept of *deblurring* event frames such that learning algorithms trained on simulated data can generalize to real scenes.
- Conception of segmentation flow using EVSegFlowNet to obtain both segmentation and optical flow in a single network.
- Control Policy based on estimated motion of multiple IMOs under various scenarios.

#### D. Organization of the paper:

The organization of the paper is structured around the development of three networks, namely, *EVDeBlurNet*,

*EVHomographyNet* and *EVSegFlowNet*. Because the data we use for training has little to no noise while the real data we use for testing has a lot of blur and noise, we need to deblur and denoise the event image sequences before any computation takes place. This is accomplished by the *EVDeBlurNet* (Sec. II-A). An approximation of the background motion (ego-motion) is obtained using data from a downfacing event camera through the *EVHomographyNet* (Sec. II-B), and the *EVSegFlowNet* (Sec. II-C) is the network that learns to segment the IMOs and compute their image motion. All networks come together to feed into the control scheme for dodging (Sec. III). We also bring into limelight the generality of our perception stack in Sec. III-D by extending the approach to the problem of pursuit. IV illustrates the experimental setup and provides error analyses of the approaches presented along with detailed ablation studies. We finally conclude the paper in Sec. V with parting thoughts on future work.

### E. Problem Formulation and Proposed Solutions

A quadrotor moves in a static scene with multiple independently moving dynamic objects/obstacles/IMOs. The quadrotor is equipped with a front facing event camera, a downfacing lower resolution event camera coupled with sonar for altitude measurements and an Inertial Measurement Unit (IMU). The problem we address is as follows: *Can we present a scalable AI framework for the task of dodging/evading/avoiding these dynamic obstacles without any prior knowledge about the obstacles, using only onboard sensing and computation?* We present various flavors of the dodging problem, hovering quadrotor dodging unknown obstacles, slow-moving quadrotor dodging unknown shaped obstacles given a bound on size, hovering and slow moving quadrotor dodging known objects (particularly targeted to spherical objects of known radii). We also broaden the horizon of our approach by demonstrating pursuit/intercept of a known object using the same AI framework showcasing that our proposed framework can be used in a general navigation stack on a quadrotor and can be re-purposed for various related tasks by adapting the control strategy.

### F. Coordinate Frames

The letters  $I$ ,  $E^F$ ,  $E^D$ ,  $S$  and  $W$  denote coordinate frames on the Inertial Measurement Unit (IMU), front facing event camera, down facing event camera, down facing sonar and the world respectively (Fig. 4). All the sensors are assumed to be rigidly attached with the intrinsic and extrinsic calibration between them known. A pinhole camera model is used for the formation of the image. The world point  $\mathbf{X}$  gets projected onto the image plane point  $\mathbf{x}$ . Unless otherwise stated, the points on the image plane are used after rectification.

## II. EMBODIED AI BASED NAVIGATION STACK

An overview of our proposed approach is illustrated in Fig. 3.

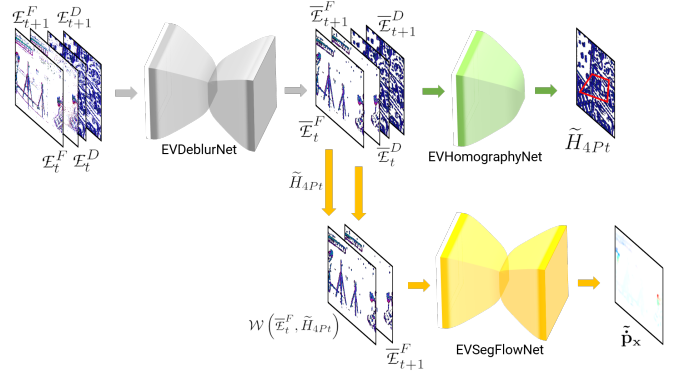


Fig. 3. Overview of the proposed neural network based navigation stack for the purpose of dodging.

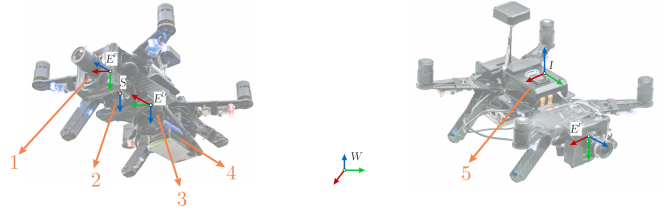


Fig. 4. Representation of coordinate frames on the hardware platform used. (1) Front facing DAVIS 240C, (2) down facing sonar on PX4Flow, (3) down facing DAVIS 240B, (4) NVIDIA TX2 CPU+GPU, (5) Intel® Aero Compute board.

### A. EVDeBlurNet

We collect the events within a time interval and represent the data as an image, the event frame  $\mathcal{E}$  (refer to Section S.I. Though event representation offers many advantages regarding computational complexity and providing tight time bounds on operation, there is a hitch. Event frames can be “blurry” based on a combination of the integration time  $\delta t$ , apparent scene movement on the image plane (which depends on the amount of camera movement and depth of the scene) and scene contrast (contrast of the latent image pixels). Here, we define blur on the event frame  $\mathcal{E}$  as the event triggers from the same point on the world not being aligned on the image plane in a small integration time  $\delta t$  due to the way events are triggered on the sensor and accumulated in our formulation. An event is triggered when the relative contrast (on the latent image  $I$ ) exceeds a threshold  $\tau$  and is mathematically modelled as

$$\|\log(I)\|_1 \approx \|\langle \nabla_{\mathbf{x}} \log(I), \dot{\mathbf{x}} \Delta t \rangle\|_1 \geq \tau$$

Here,  $\nabla_{\mathbf{x}}$  is the spatial gradient,  $\dot{\mathbf{x}}$  is the motion field on the image and  $\Delta t$  is the time since the previous event at the same location. The above equation elucidates how the latent image contrast, motion and depth are coupled to event frames. Note that,  $\dot{\mathbf{x}}$  depends on the 3D camera motion and the scene depth. We refer the reader to [10] for more details.

This “blurriness” of the event frame can adversely affect the performance of algorithms built on them. To alleviate this problem, we need to deblur the event images. This is fairly easy if we directly use the spatio-temporal event

cloud and follow the approach described in [11]. Essentially the problem deals with finding point trajectories along the spatio-temporal point cloud to maximize a heuristically chosen contrast function. Mathematically, we want to solve the following problem.

$$\operatorname{argmax}_{\theta} \mathcal{C}(\mathcal{W}(\mathcal{E}, \theta))$$

where  $\mathcal{C}$  is a heuristic contrast function and  $\theta$  are the parameters of point trajectories in the spatio-temporal point cloud according to which the events are warped and  $\mathcal{W}(\mathcal{E}, \theta)$  represents the event image formed by the warped events. In our scenario, we want to model the deblurring problem in 2D, i.e., working on  $\mathcal{E}$  directly without the use of a spatio-temporal point cloud so that the problem can be solved efficiently using a 2D Convolutional Neural Network (CNN). Such a deblurring problem using a single image has been studied extensively for traditional cameras for rectifying motion blurred photos. Our modified problem in 2D can be formulated as:

$$\operatorname{argmax}_{\mathcal{K}} \mathcal{C}(\mathcal{K} \circledast \mathcal{E})$$

Here  $\mathcal{K}$  is the heterogeneous deblur kernel and  $\circledast$  is the convolution operator. However, estimating  $\mathcal{K}$  directly is not constrained enough to be learned in an unsupervised manner. Instead, we formulate the deblurring problem inspired by Total Variation (TV) denoising to give us the final optimization problem as follows:

$$\operatorname{argmax}_{\overline{\mathcal{E}}} \mathcal{C}(\overline{\mathcal{E}}) + \lambda \operatorname{argmin}_{\overline{\mathcal{E}}} \mathcal{D}(\mathcal{E}, \overline{\mathcal{E}})$$

where  $\overline{\mathcal{E}}$  represents the deblurred event frame,  $\lambda$  is a regularization penalty and  $\mathcal{D}$  represents a distance function to measure similarity between two event frames. Note that directly solving  $\operatorname{argmax}_{\overline{\mathcal{E}}} \mathcal{C}(\overline{\mathcal{E}})$  yields trivial solutions of high frequency noise.

To learn the function using a neural network we convert the  $\operatorname{argmax}$  operator into an  $\operatorname{argmin}$  operator as follows:

$$\operatorname{argmin}_{\overline{\mathcal{E}}} -\mathcal{C}(-\overline{\mathcal{E}}) + \lambda \mathcal{D}(\mathcal{E}, \overline{\mathcal{E}})$$

Intuitively, the higher the value of the contrast, the lower the value of the loss function, but going away too far from the input will penalize the loss function striking a balance between high contrast and similarity to the input image. We call our CNN which generates the deblurred event images *EVDeBlurNet*. It takes as input  $\mathcal{E}$  and outputs deblurred  $\overline{\mathcal{E}}$ . The network architecture is a simple Encoder Decoder with four convolutional and four deconvolutional layers with batch normalization (Supplementary material Section S.III). Another benefit which can be intuited due to the encoder decoder's lossy reconstruction is that it removes stray events which are generally noise and retains only events corresponding to contours of real-world scene objects or strong edges and this greatly increases the signal to noise ratio.

## B. EVHomographyNet

A very simple and computationally inexpensive way to obtain odometry on a quadrotor is to use a downfacing camera and assume that the real world patch the downfacing camera is looking at is well approximated by a plane. This approximation coupled with data from an IMU and a distance sensor enables high speed “cheap” odometry for navigation. Though a lot of optical flow sensors based on traditional cameras exist, there are none based on the event based cameras because of the lack of open-source efficient algorithms for homography estimation. We propose the first deep learning based solution to this problem which can be run on an embedded computer at reasonably high speeds and good accuracy. Let us mathematically formulate our problem. Let  $\mathcal{E}_t$  and  $\mathcal{E}_{t+1}$  be the event frames captured at times  $t$  and  $t+1$ , respectively, and  $\delta t \ll \Delta t$  where  $\Delta t$  is the time difference between the start times of event frame accumulation. We assumed that the patch which the downfacing camera is looking at can be well approximated by a plane. This could be because of a small field of view of the camera or because of the quadrotor flying high in the air or due to the world being actually flat like an empty floor. This condition constraint the transformation between the two events frames to a homography. This can be written as  $\mathbf{x}_{t+1} = \mathbf{H}_t^{t+1} \mathbf{x}_t$ , where  $\mathbf{x}_{t+1}, \mathbf{x}_t$  represent the homogeneous point correspondences in the two event frames and  $\mathbf{H}_t^{t+1}$  is the resulting non-singular  $3 \times 3$  homography matrix between the two frames. We follow the previous works on deep learning based homography estimation [12] [13] to implement both supervised and unsupervised flavors of deep learning based homography estimation. For the supervised flavor of the algorithm, we generate synthetic homography warped event frames and train them using the following loss function.

$$\operatorname{argmin}_{\tilde{H}_{4Pt}} \mathbb{E} \left( \|\tilde{H}_{4Pt} - \hat{H}_{4Pt}\|_2 \right)$$

Here  $\tilde{H}_{4Pt}$  and  $\hat{H}_{4Pt}$  are the predicted and ground truth 4-point homographies. We refer the readers to [14] for more details.

For the unsupervised version, we adapt the mathematical formulation [13] for TensorDLT and the Spatial Transformer Network (STN) using bilinear interpolation. The final loss function is given as:

$$\operatorname{argmin}_{\tilde{H}_{4Pt}} \mathbb{E} \left( \mathcal{D} \left( \mathcal{W}(\mathcal{E}_t, \tilde{H}_{4Pt}), \mathcal{E}_{t+1} \right) \right)$$

Here  $\mathcal{W}$  is a generic differentiable warp function and can take on different mathematical formulations based on its second argument (model parameters). In this case  $\mathcal{W}$  contains both the TensorDLT and the STN. As before,  $\mathcal{D}$  represents a distance measuring image similarity between two event frames (Refer to the supplementary material Section S.II for the mathematical formulations of  $\mathcal{D}$ ).

### C. EVSegFlowNet

The end goal of this work is to detect/segment Independently Moving Objects (IMOs) and to dodge them. One could fragment this problem into two major parts, detecting IMOs, and subsequently estimating their motion to issue a control command to move away from the IMO in a safe manner. Let's start by discussing each fragment. Firstly, we want to segment the object using consecutive event frames  $\mathcal{E}_t$  and  $\mathcal{E}_{t+1}$ . A simple way to accomplish this is by generating simulated data with known segmentation for each frame and then training a CNN to predict the foreground (IMO)/background segmentation. Such a CNN can be trained using a simple cross entropy loss function as shown below.

$$\operatorname{argmin}_{p_f} -\mathbb{E}(\mathbb{1}_f \log(p_f) + \mathbb{1}_b \log(p_b))$$

Here,  $\mathbb{1}_f, \mathbb{1}_b$  are the indicator variables denoting if a pixel belongs to foreground or background. They are mutually exclusive, i.e.,  $\mathbb{1}_f = \neg \mathbb{1}_b$  and  $p_f, p_b$  represent the foreground and background predicted probabilities where  $p_f + p_b = 1$ . Note that each operation in the above equation is performed per pixel, and then an average over all pixels is computed. In the second step we want to estimate the IMO motion. Without any prior knowledge about the IMO it is impossible to estimate the 3D motion of the IMO from a monocular camera (event based or traditional). To make this problem tractable, we assume a prior about the object. More details can be found in Subsection III.

Once we have a prior about the object, we can estimate the 3D IMO motion using optical flow of the pixels corresponding to the IMO on the image plane. A simple way to obtain optical flow is to train a CNN in a supervised manner. However, recent research has shown that these do not generalize well to new scenes/objects [15]. A better way is to use a self-supervised or completely unsupervised loss function.

$$\operatorname{argmin}_{\hat{\mathbf{x}}} \mathbb{E}(\mathcal{D}(\mathcal{W}(\mathcal{E}_t, \hat{\mathbf{x}}), \mathcal{E}_{t+1}))$$

Here  $\hat{\mathbf{x}}$  is the estimated optical flow between  $\mathcal{E}_t \mapsto \mathcal{E}_{t+1}$  and  $\mathcal{W}$  is a differentiable warp function based on optical flow and bilinear interpolation implemented using an STN. The self-supervised flavor of this algorithm [15] utilizes corresponding image frames instead of event frames for the loss function but the input is still the stack of event frames. One could utilize the two networks we talked about previously and solve the problem of dodging, however, one would need to run two neural networks for this purpose. Furthermore, this method suffers from a major problem: any unsupervised or self-supervised method can estimate rigid optical flow (optical flow corresponding to the background regions  $\mathcal{B}$ ) accurately but the non-rigid optical flow (optical flow corresponding to the foreground regions  $\mathcal{F}$ ) is not very accurate. This is an artifact because of the number of pixels corresponding to the foreground is often far less than that corresponding to the background, i.e.,  $|\mathcal{F}| \ll |\mathcal{B}|$ . One would have to train for a lot of iterations to obtain accurate optical

flow results on these foreground pixels which runs into the risk of overfitting to the dataset. This defeats the promise of self-supervised or unsupervised formulations.

To solve both the problems of complexity and accuracy, we formulate the problem using a semi-supervised approach to learn segmentation and optical flow at the same time, which we call *EVSegFlowNet*. We call the output of the network *segmentation flow* denoted by  $\tilde{\mathbf{p}}$  which is defined as follows.

$$\tilde{\mathbf{p}}_{\mathbf{x}} = \begin{cases} \tilde{\mathbf{p}}_{\mathbf{x}}, & \text{if } \mathbb{1}_f(\mathbf{x}) = 1 \\ \mathbf{0}, & \text{if } \mathbb{1}_b(\mathbf{x}) = 1 \end{cases}$$

One could intuit that we can obtain a noisy segmentation for free by simple thresholding on the magnitude of  $\tilde{\mathbf{p}}_{\mathbf{x}}$ . To utilize the network to maximum capacity the input to the network is the ego-motion/odometry based warped event frame such that the background pixels in the two input event frames are almost aligned and the only misalignment comes from the IMOs. This ensures that the network's capacity can be utilized fully for learning sub-pixel accurate optical flow for IMO regions. The input to the EVSegFlowNet is  $\mathcal{W}(\mathcal{E}_t, \tilde{H}_{4Pt})$  and  $\mathcal{E}_{t+1}$ . Here,  $\tilde{H}_{4Pt}$  is transformed to  $E^F$  before warping.

A complexity analysis of EVSegFlowNet is given in Section S.VI of the supplementary material. The success of our approach can be seen from the experimental results. The loss function for learning  $\tilde{\mathbf{p}}_{\mathbf{x}}$  is given below.

$$\operatorname{argmin}_{\tilde{\mathbf{p}}_{\mathbf{x}}} \mathbb{E}(\mathcal{D}(\mathcal{W}(\mathcal{E}'_t, \tilde{\mathbf{p}}_{\mathbf{x}}) \circ \mathbb{1}_f, \mathcal{E}_{t+1} \circ \mathbb{1}_f)) + \lambda_1 \mathbb{E}(\|\tilde{\mathbf{p}}_{\mathbf{x}} \circ \mathbb{1}_b\|_1) + \lambda_2 \mathbb{E}(\|\tilde{\mathbf{p}}_{\mathbf{x}} \circ \mathbb{1}_b\|_2^2)$$

Here,  $\lambda_1$  and  $\lambda_2$  are regularization parameters. This loss function is essentially the image difference with elastic net like regularization penalty. This penalty makes the network make background flow zero fairly quickly as compared to simple  $l_1$  or quadratic penalty whilst being robust to outliers (errors in segmentation mask creation).

### III. CONTROL POLICY FOR DODGING DYNAMIC OBSTACLES

In this section, we present a solution for evading multiple known and/or unknown IMOs.

Let us consider three different flavors of IMOs: (a) Sphere with known radius  $r$ , (b) Unknown shaped objects with known bound on the size and (c) Unknown objects with no prior knowledge. We tackle each of these cases differently. Knowing the prior information about the geometric nature helps us achieve much more robust results and fine-grain control.

We define  $\mathcal{F}$  as the projection of all the IMOs on the image plane such that  $\mathcal{F} = \bigcup_{\forall i} \mathcal{F}_i$ , where  $\mathcal{F}_i$  denotes the  $i^{\text{th}}$  IMO's image plane projection. Now, let's confabulate each flavor of the problem separately in the following subsections.

### A. Sphere with known radius $r$

Let us first begin with the simplest case, i.e., a *single spherical IMO with known radius  $r$* . On a rectified image the projection of a sphere on the image plane is an ellipse [16]. Evading such an object under no gravitational influence has been tackled and well analyzed by [17]. For spherical objects under the gravitational influence, we estimate the initial 3D position using the known radius information and then we track the object over a few  $\mathcal{E}$  to obtain the initial 3D velocity. Here, the tracking is done by detection (segmentation) on every frame.

Assuming a classical physics model, we predict the future trajectory  $\mathbf{X}_i^{\text{IMO}}$  of the sphere when it is only under the influence of gravity. Now, we define the point  $\mathbf{X}_{i,p}^{\text{IMO}}$  as the intersection of the trajectory  $\mathbf{X}_i^{\text{IMO}}$  and the image plane. For the case of a single spherical IMO, we compute the distance between  $\mathbf{X}_{i,p}^{\text{IMO}}$  and the initial position of the quadrotor  $O$ , denoted by vector  $\mathbf{x}_{\min} \in \mathbb{R}^{2 \times 1}$ . The “safe” direction is represented as  $\mathbf{x}_s = -\mathbf{x}_{\min}$ . A simple Proportional-Integral-Derivative (PID) controller based on the differential flatness model of the quadrotor is used with high proportional gain for a quick response to move in the direction  $\mathbf{x}_s$ . The minimum amount of movement is equal to the extended obstacle size (the size of the quadrotor is added to the object size).

Now, let’s extend to the evasion of *multiple spherical IMOs*. We assume that while objects are detected, there is no occlusion among different IMOs in the front event camera frame. Then, each object  $\mathcal{F}_i$  is segmented using mean shift clustering. For each object  $\mathcal{F}_i$ , the 3D position and velocity are estimated. It is important to note that since all the objects were targeted at the quadrotor, they are bound to intercept the image plane, say at point  $\mathbf{X}_{i,p}^{\text{IMO}}$  (Fig. 5). For evading multiple objects, the quadrotor moves in  $\mathbf{x}_s$  direction in the image plane such that  $\mathbf{x}_s = (\mathbf{X}_{i,p}^{\text{IMO}} + \mathbf{X}_{i+1,p}^{\text{IMO}})$ , where  $(\mathbf{X}_{i,p}^{\text{IMO}}, \mathbf{X}_{i+1,p}^{\text{IMO}})$  is a consecutive cyclic pair of vectors for which we solve the following optimization problem:

$$\underset{\mathbf{X}_{i,p}^{\text{IMO}}, \mathbf{X}_{i+1,p}^{\text{IMO}}}{\operatorname{argmin}} \left\langle \frac{\mathbf{X}_{i,p}^{\text{IMO}}}{\|\mathbf{X}_{i,p}^{\text{IMO}}\|_2}, \frac{\mathbf{X}_{i+1,p}^{\text{IMO}}}{\|\mathbf{X}_{i+1,p}^{\text{IMO}}\|_2} \right\rangle$$

where  $\langle \cdot, \cdot \rangle$  denotes the inner product/dot product between two vectors. In this case, the size of the biggest IMO is used to execute the control policy as before.

### B. Unknown shaped objects with bound on size

Now, consider the case of evading an IMO of an arbitrary shape  $\mathcal{S}$ . As the projection of  $\mathcal{S}$  on the image plane can be either convex or non-convex, we first obtain the convex hull of  $\mathcal{S}$  denoted by  $\mathcal{H}$ . Clearly, an evasive maneuver performed using  $\mathcal{H}$  guarantees evasion from the object when the rotation of the IMO with respect to the camera is small.

Next, we find the principle axes of the projection of  $\mathcal{H}$  on the image plane. Because we have a bound on size, i.e., we have a bound on the length of the maximum principle axis in 3D, we can evade this object assuming it to be a sphere of this diameter. Note that this method is more conservative

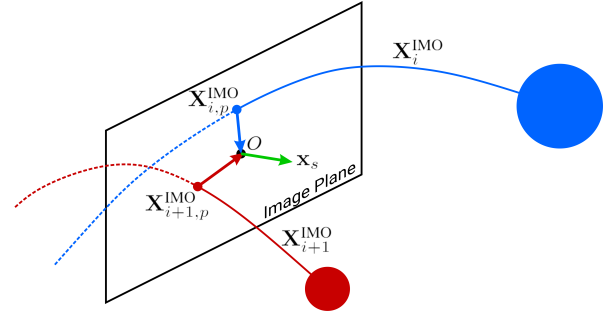


Fig. 5. Vectors  $\mathbf{X}_{i,p}^{\text{IMO}}$  and  $\mathbf{X}_{i+1,p}^{\text{IMO}}$  represent the intersection of the trajectory and the image plane.  $\mathbf{x}_s$  is the direction of the “safe” trajectory. All the vectors are defined with respect to the center of the quadrotor projected on the image plane,  $O$ . Both of the spheres are of known radii.

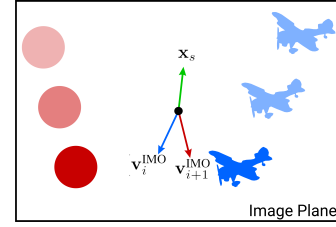


Fig. 6. Representation of velocity direction of multiple unknown IMOs. The vector  $\mathbf{v}_i^{\text{IMO}}$  and  $\mathbf{v}_{i+1}^{\text{IMO}}$  represent velocities of the corresponding objects.  $\mathbf{x}_s$  denotes the “safe” direction for the quadrotor.

than the previous approach constraining the sensing range and latency based on how close the bound is to actual object size.

### C. Unknown objects with no prior knowledge

Without any prior knowledge about the object, it is geometrically infeasible to obtain the 3D velocity of an IMO using a monocular camera. However, we can predict a possible safe trajectory  $\mathbf{x}_s$  depending on the velocity direction of the IMOs on the image plane. We compute the unit vector  $\mathbf{v}_i^{\text{IMO}}$  in which the IMO is moving by tracking the segmentation mask of the IMO or by computing the mean optical flow direction of the region of interest. For a single unknown IMO, a heuristic is chosen such that the quadrotor moves in the direction perpendicular to the velocity of the IMO on the image plane, i.e., a safe direction for the quadrotor motion which satisfies  $\langle \mathbf{x}_s, \mathbf{v}_i^{\text{IMO}} \rangle = 0$ .

For evading multiple unknown IMOs, the quadrotor moves in  $\mathbf{x}_s$  direction in the image plane such that  $\mathbf{x}_s = -(\mathbf{v}_i^{\text{IMO}} + \mathbf{v}_{i+1}^{\text{IMO}})$ , where  $(\mathbf{v}_i^{\text{IMO}}, \mathbf{v}_{i+1}^{\text{IMO}})$  is a consecutive cyclic pair of unit vectors found by solving the following optimization problem (Fig. 6).

$$\underset{\mathbf{v}_i, \mathbf{v}_{i+1}}{\operatorname{argmin}} \langle \mathbf{v}_i, \mathbf{v}_{i+1} \rangle$$

Note that, we don’t have an estimate of how much to move so as to evade the object. Practically, we move as far as possible in the hope of evading the obstacles. *Clearly, there is no guarantee of avoiding the IMO in this case and it will depend on the sensing range and latency.*



Fig. 7. Objects used in experiments. Left to right: Airplane, car, spherical ball and Bebop 2.

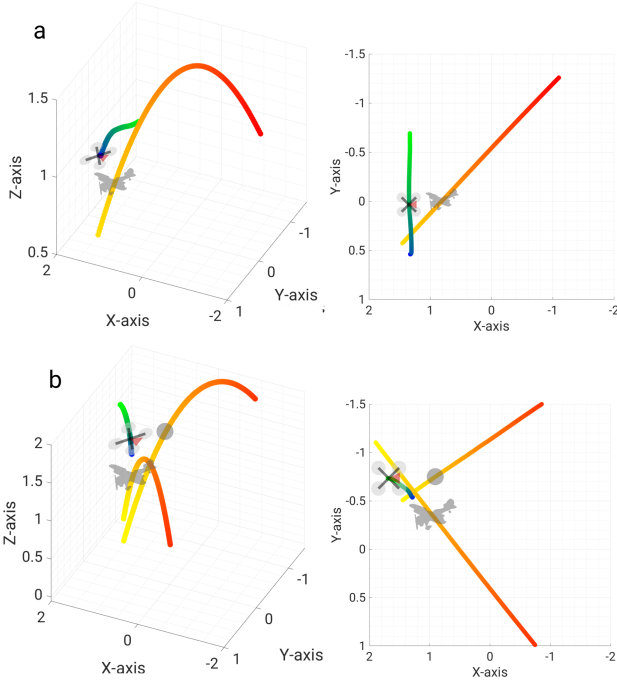


Fig. 8. Vicon estimates for the trajectories of the objects and quadrotor. (a) Perspective and top view for single unknown object case, (b) perspective and top view for multiple object case. Object and quadrotor silhouettes are shown to scale. Time progression is shown from red to yellow for objects and blue to green for the quadrotor.

#### D. Pursuit: A reversal of evasion?

The generality of our perception stack for navigation is demonstrated by showing that pursuit can be accomplished using a simple reversal of the control policy for the cases presented in III-A and III-B.

Additionally, for an IMO which is self-propelled like a quadrotor, one can perform both pursuit and evade tasks by assuming a linear motion model. Note that here no concept of the agent's intent is used but it can be introduced with an additional neural network for predicting the motion model of the agent (intent) [18]. We leave this for future work.

In the next section, we provide a detailed experimental analysis and present our results for all the aforementioned cases.

## IV. EXPERIMENTS

### A. Experimental Setup

A detailed description of the hardware setup is given in Section S.V of the supplementary material.

The experiments were conducted in the Autonomy Robotics and Cognition (ARC) lab's indoor flying space at the University of Maryland, College Park. The total flying volume is about  $6 \times 5.5 \times 3.5 \text{ m}^3$ . A Vicon motion capture system with 8 vantage V8 cameras are used to obtain ground truth at 100 Hz. The objects were either thrown or flown (in-case of the bebop experiment) at the quadrotor during hover or slow flight (simulating slow drift) at speeds ranging from  $4.4 \text{ ms}^{-1}$  to  $6.8 \text{ ms}^{-1}$  from a distance ranging from 3.6 m to 5.2 m. To enable robust homography estimation, we laid down carpets of different textures on the ground to obtain strong contours in event frames (Refer to supplementary Fig. S6).

We used four different objects in our experiments, (a) a spherical ball of diameter 140 mm, (b) a car of size  $185 \times 95 \times 45 \text{ mm}$  (here a bound of 240 mm is used), (c) an airplane of size  $270 \times 250 \times 160 \text{ mm}$  (size information not used in experiments), (d) a Bebop 2 of size  $330 \times 380 \times 200 \text{ mm}$ . Also, we used an integration time  $\delta t$  of 30 ms for all our experiments.

### B. Experimental Results and Discussion

In this paper, we considered the case of navigating through different sets of multiple dynamic obstacles. We dealt with six different evading combinations and one pursuit experiment: (a) Spherical ball with a known radius of 140 mm, (b) car with a bound on the maximum dimension size of 240 mm, (c) airplane with no prior information, (d) Bebop 2 flying at a constant velocity, (e) multiple unknown objects, (f) pursuit of Bebop 2 and (g) low-light dodging experiment. For each evasion case, the objects are directly thrown towards the Aero quadrotor such that a collision would definitely occur if the Aero holds its initial position. The objects used in the experiments are shown in Fig. 7. For each case, a total of 30 trials were conducted. The Vicon plots for cases (c) and (e) are shown in Fig. 8. Notice that the objects would have hit the quadrotor if it had not moved from its initial position. We achieved a remarkable success rate of 86% in cases (a) and (b), 76% in case (c). Both Parrot Bebop 2 experiments (case (d), (f)) resulted in 83% success rate. Case (e) was carefully performed with synchronized throws between the two objects and resulted about 76% success rate. For the low-light experiment (case (g)), we achieved a success rate of 70%. Here success is defined as both a successful detection and evasion for the evade experiments and both a successful detection and collision for the pursuit task. Fig. 9 shows sequences of images for cases (a)-(f) along with sample front facing event frame and segmentation outputs.

Before the IMO is thrown at the quadrotor, the quadrotor maintains its position (hover) using the differential  $X^W$  and  $Y^W$  estimates from the EVHomographyNet and  $Z^W$  estimates from the sonar.

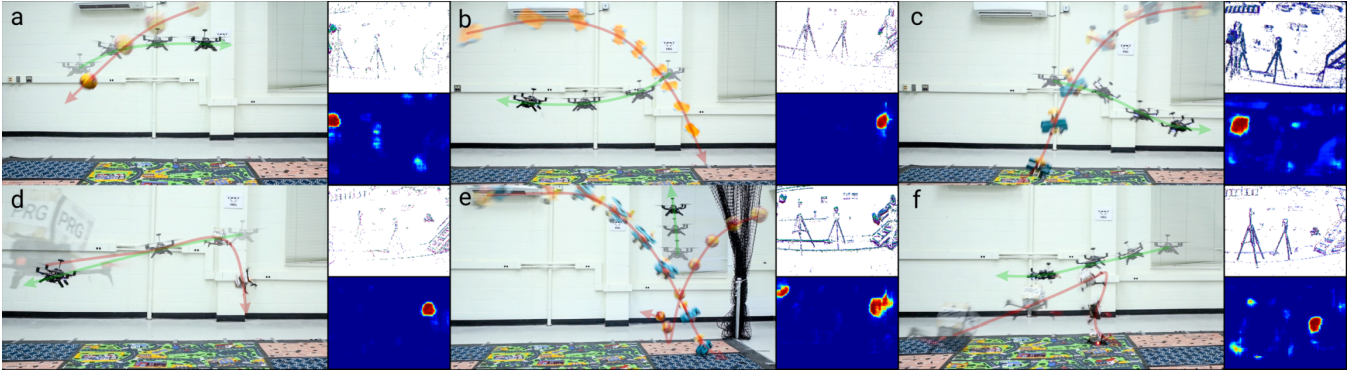


Fig. 9. Sequence of images of quadrotor dodging or persuading of objects. (a)-(d): Dodging a spherical ball, car, airplane and Bebop 2 respectively. (e): Dodging multiple objects simultaneously. (f): Pursuit of Bebop 2 by reversing control policy. Object and quadrotor transparency show progression of time. Red and green arrows indicate object and quadrotor directions respectively. On-set images show front facing event frame (top) and respective segmentation obtained from our network (down).

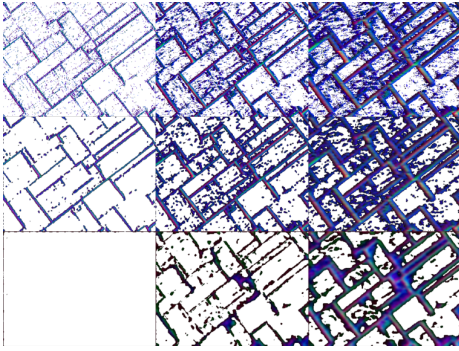


Fig. 10. Output of EVDeBlurNet for different integration time and loss functions. Top row: raw event frames, middle row: deblurred event frames with  $\mathcal{D}_2$  and bottom row: deblurred event frames with  $\mathcal{D}_3$  with  $\delta t$ . Left to right:  $\delta t$  of 1 ms, 5 ms and 10 ms. Notice that only the major contours are preserved and blurred contours are thinned in deblurred outputs.

When the IMO is thrown at the quadrotor, the IMO is detected for five consecutive frames to estimate either the trajectory or image plane velocity and to remove outliers using simple morphological operations. This gives a perception response lag of 60 ms (each consecutive frame pair takes 10 ms for the neural network computation and 2 ms for the post-processing). Finally, the quadrotor moves using the simple PID controller presented before.

Note that, we talked about obtaining both segmentation and optical flow from EVSegFlowNet. This was based on the conceptualization of optical flow being used for other tasks as well. However, if only the dodging task is to be performed, a smaller segmentation network can be used without much loss of accuracy.

Fig. 10 shows the input and output of EVDeBlurNet for losses  $\mathcal{D}_2$  and  $\mathcal{D}_3$  under  $\delta t = \{1, 5, 10\}$  ms. Observe the amount of noise (stray events not associated with strong contours) in the raw images (top row of Fig. 10). The second row shows the output of DeBlurNet for  $\mathcal{D}_2$  loss. Observe that this works well for smaller integration times but for larger integration times, the amount of denoising and deblurring performance deteriorates. However,  $\mathcal{D}_3$  loss which is aimed

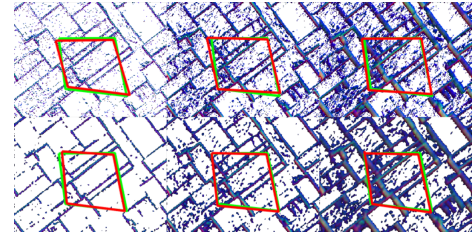


Fig. 11. Output of EVHomographyNet for raw and deblurred event frames at different integration times. Green and red color denotes ground truth and predicted  $\hat{H}_{APt}$  respectively. Top row: raw events frames and bottom row: deblurred event frames. Left to right:  $\delta t$  of 1 ms, 5 ms and 10 ms. Notice that the deblurred homography outputs are almost not affected by integration time.

at outlier rejection is more suppressive of weak contours and hence one can observe that the frame has almost no output for smaller integration times. This has the effect of working well for larger integration times.

Fig. 11 shows the output of EVHomographyNet using the supervised loss function on both raw (top row) and deblurred frames (bottom row). Observe that the deblurred homography estimation is more robust to changes in different integration times. Table I shows the quantitative evaluation of different methods used for training EVHomographyNet. Here,  $RMSE_i$  and  $RMSE_o$  denote the average root mean square error [13] in the testing dataset with textures similar to that of the training set, and completely novel textures respectively.  $RMSE_o$  quantifies how well the network can generalize to unseen samples. Notice that the supervised flavors of the algorithm work better (lower  $RMSE_i$  and  $RMSE_o$ ) than their respective unsupervised counterparts. We speculate that this is because of the sparsity in data and that the simple image based similarity metrics not being well suited for event frames. We leave crafting a novel loss function for event frames as a potential avenue for future work. Also, notice how deblur variants of the algorithms almost always work better than their respective non-deblurred counterparts highlighting the utility of EVDeblurNet.

Table II shows the quantitative results of different

TABLE I  
QUANTITATIVE EVALUATION OF DIFFERENT METHODS FOR HOMOGRAPHY ESTIMATION.

| Method (Loss)               | RMSE <sub>i</sub> in px. |                       |                        |                        |                        | RMSE <sub>o</sub> in px. |                       |                        |                        |                        |
|-----------------------------|--------------------------|-----------------------|------------------------|------------------------|------------------------|--------------------------|-----------------------|------------------------|------------------------|------------------------|
|                             | $\gamma = \pm[0, 5]$     | $\gamma = \pm[6, 10]$ | $\gamma = \pm[11, 15]$ | $\gamma = \pm[16, 20]$ | $\gamma = \pm[21, 25]$ | $\gamma = \pm[0, 5]$     | $\gamma = \pm[6, 10]$ | $\gamma = \pm[11, 15]$ | $\gamma = \pm[16, 20]$ | $\gamma = \pm[21, 25]$ |
| Identity                    | 3.92 $\pm$ 0.83          | 11.40 $\pm$ 0.70      | 18.43 $\pm$ 0.70       | 25.50 $\pm$ 0.70       | 32.55 $\pm$ 0.71       | 3.92 $\pm$ 0.84          | 11.40 $\pm$ 0.70      | 18.44 $\pm$ 0.71       | 25.49 $\pm$ 0.70       | 32.55 $\pm$ 0.71       |
| S                           | 3.23 $\pm$ 1.13          | 3.90 $\pm$ 1.34       | 5.31 $\pm$ 2.05        | 9.63 $\pm$ 4.57        | 17.65 $\pm$ 7.00       | 4.15 $\pm$ 1.78          | 5.05 $\pm$ 2.19       | 6.99 $\pm$ 3.11        | 11.21 $\pm$ 4.84       | 18.37 $\pm$ 6.61       |
| US* ( $\mathcal{D}_1$ )     | 2.97 $\pm$ 1.22          | 3.84 $\pm$ 1.61       | 5.99 $\pm$ 2.78        | 11.64 $\pm$ 5.69       | 20.36 $\pm$ 7.68       | 3.92 $\pm$ 1.53          | 5.31 $\pm$ 2.43       | 8.14 $\pm$ 3.86        | 13.63 $\pm$ 5.87       | 21.22 $\pm$ 7.35       |
| US* ( $\mathcal{D}_2$ )     | 2.48 $\pm$ 0.93          | 3.53 $\pm$ 1.43       | 5.89 $\pm$ 2.70        | 11.74 $\pm$ 5.69       | 20.51 $\pm$ 0.70       | 3.19 $\pm$ 1.26          | 4.86 $\pm$ 2.31       | 7.92 $\pm$ 3.73        | 13.47 $\pm$ 5.71       | 21.22 $\pm$ 7.08       |
| DB + S                      | 2.73 $\pm$ 1.01          | 3.16 $\pm$ 1.23       | 4.00 $\pm$ 1.79        | 6.50 $\pm$ 3.54        | 12.22 $\pm$ 6.58       | 3.69 $\pm$ 1.51          | 4.49 $\pm$ 2.10       | 5.91 $\pm$ 3.16        | 9.04 $\pm$ 4.90        | 14.60 $\pm$ 6.95       |
| DB + US ( $\mathcal{D}_1$ ) | 2.19 $\pm$ 0.88          | 3.04 $\pm$ 1.57       | 4.99 $\pm$ 2.75        | 10.16 $\pm$ 5.54       | 18.62 $\pm$ 7.85       | 3.08 $\pm$ 1.37          | 4.63 $\pm$ 2.68       | 7.57 $\pm$ 4.30        | 13.16 $\pm$ 6.25       | 21.08 $\pm$ 7.81       |
| DB + US ( $\mathcal{D}_2$ ) | 2.41 $\pm$ 1.06          | 3.30 $\pm$ 1.77       | 5.36 $\pm$ 3.02        | 10.39 $\pm$ 5.78       | 18.77 $\pm$ 8.07       | 3.35 $\pm$ 1.76          | 5.05 $\pm$ 3.03       | 8.11 $\pm$ 4.65        | 13.46 $\pm$ 6.48       | 21.08 $\pm$ 7.81       |

\* Trained for 100 epochs on supervised and then fine-tuned on unsupervised for 100 more epochs.  $\gamma$  denotes the perturbation range in px. for evaluation.

TABLE II  
QUANTITATIVE EVALUATION OF DIFFERENT METHODS FOR  
SEGMENTATION OF IMO.

| Method              | DR <sub>i</sub> | DR <sub>o</sub> | Run Time | FLOPs | Num. Params |
|---------------------|-----------------|-----------------|----------|-------|-------------|
| (Loss)              | in %            | in %            | in ms    | in M  | in M        |
| SegNet              | 40.4            | 49.0            | 1.5      | 222   | 0.03        |
| DB + SegNet         | 68.7            | 81.5            | 7.5      | 4900  | 2.33        |
| DB + H + SegNet     | 69.1            | 83.2            | 10       | 5150  | 3.63        |
| SegFlowNet          | 81.9            | 88.3            | 1.5      | 222   | 0.03        |
| DB + SegFlowNet     | 90.1            | 93.3            | 7.5      | 4900  | 2.33        |
| DB + H + SegFlowNet | 90.7            | 93.4            | 10       | 5150  | 3.63        |

variants of segmentation networks trained using the  $\mathcal{D}_2$  loss for SegFlowNet. Here DB denotes the deblurred outputs produced using the combination of  $\mathcal{D}_2$  and  $\mathcal{C}_2$  loss. Also, H denotes the stack of warped  $\mathcal{E}_t$  and  $\mathcal{E}_{t+1}$  using the outputs of the network DB + S in Table I. Here DR denotes the detection rate and is defined as:

$$\text{DR} = \mathbb{E} \left( \frac{(\overline{(\mathcal{D} \cap \mathcal{G}) \circ \mathbb{I}_{\mathcal{E}}})}{(\overline{\mathcal{G} \circ \mathbb{I}_{\mathcal{E}}})} \geq \tau \right) \times 100\%$$

where  $\mathcal{G}$  and  $\mathcal{D}$  denote the ground truth and predicted masks respectively, and  $\mathbb{I}_{\mathcal{E}}$  denotes the presence of an event in either of the input event frames. For our evaluation, we choose  $\tau = 0.5$ . Notice that using both deblur and homography warping helps improve the results as anticipated. Again, DR<sub>i</sub> and DR<sub>o</sub> denote testing on trained objects and completely novel objects. As before, deblurring helps generalize much better to novel objects and deblurring with homography warping gives better results showing that the network’s learning capacity is utilized better.

The network architectures and training details are provided in the Section S.III of the supplementary material.

## V. CONCLUSIONS

We presented an AI-based algorithmic design for micro quadrotors, taking into account the knowledge of the system’s computation and timing requirements, which we call *Embodied AI*. The central conception of Embodied AI is to contrive AI building blocks which can be re-purposed. This philosophy was used to develop a method to dodge dynamic obstacles using only a monocular event camera and onboard sensing. To our knowledge, this is the first deep learning based solution to the problem of dynamic obstacle avoidance using event cameras on a quadrotor. We also show the generalizability of our navigation stack by extending

our work to the pursuit task. As a parting thought, a better similarity scoring metric between event frames or a more robust construction of event frames can improve our results.

## ACKNOWLEDGEMENT

This work was partly funded by the Brin Family Foundation, National Science Foundation under grant BCS 1824198, ONR under grant N00014-17-1-2622, the Northrop Grumman Mission Systems University Research Program. The authors would like to thank NVIDIA for the grant of an NVIDIA Titan-Xp GPU and Intel for the grant of the Intel Aero Platform.

## REFERENCES

- [1] Nitin J. Sanket et al. GapFlyt: Active vision based minimalist structure-less gap detection for quadrotor flight. *IEEE Robotics and Automation Letters*, 3(4):2799–2806, Oct 2018.
- [2] John Aloimonos et al. Active vision. *International journal of computer vision*, 1(4):333–356, 1988.
- [3] Ernst Mach. *Grundlinien der Lehre von den Bewegungsempfindungen*. w. Engelmann, 1875.
- [4] Michael Bloesch et al. Robust visual inertial odometry using a direct ekf-based approach. In *2015 IEEE/RSJ international conference on intelligent robots and systems (IROS)*, pages 298–304. IEEE, 2015.
- [5] Tong Qin et al. VINS-Mono: A robust and versatile monocular visual-inertial state estimator. *IEEE Transactions on Robotics*, 34(4):1004–1020, 2018.
- [6] Huai-Jen Liang et al. SalientDSO: Bringing attention to direct sparse odometry. *IEEE Transactions on Automation Science and Engineering*, 2019.
- [7] Sean Bowman et al. Probabilistic data association for semantic SLAM. In *2017 IEEE International Conference on Robotics and Automation (ICRA)*, pages 1722–1729. IEEE, 2017.
- [8] Anton Mitrokhin, Chengxi Ye, Cornelia Fermüller, Yiannis Aloimonos, and Tobi Delbrück. Ev-imo: Motion segmentation dataset and learning pipeline for event cameras. *arXiv preprint arXiv:1903.07520*, 2019.
- [9] A. Mitrokhin et al. Event-based moving object detection and tracking. In *2018 IEEE/RSJ International Conference on Intelligent Robots and Systems (IROS)*, pages 1–9, Oct 2018.
- [10] Guillermo Gallego et al. Event-based camera pose tracking using a generative event model. *arXiv preprint arXiv:1510.01972*, 2015.
- [11] Guillermo Gallego et al. A unifying contrast maximization framework for event cameras, with applications to motion, depth, and optical flow estimation. In *The IEEE Conference on Computer Vision and Pattern Recognition (CVPR)*, June 2018.
- [12] Daniel DeTone et al. Deep image homography estimation. *arXiv preprint arXiv:1606.03798*, 2016.
- [13] Ty Nguyen et al. Unsupervised deep homography: A fast and robust homography estimation model. *IEEE Robotics and Automation Letters*, 3(3):2346–2353, 2018.
- [14] Daniel DeTone et al. Deep image homography estimation. *arXiv preprint arXiv:1606.03798*, 2016.
- [15] Alex Zhu et al. Ev-flownet: self-supervised optical flow estimation for event-based cameras. *arXiv preprint arXiv:1802.06898*, 2018.

- [16] Clarence Raymond Wylie. *Introduction to projective geometry*. Courier Corporation, 2011.
- [17] D. Falanga et al. How Fast Is Too Fast? The Role of Perception Latency in High-Speed Sense and Avoid. *IEEE Robotics and Automation Letters*, 4(2):1884–1891, April 2019.
- [18] Riccardo Spica et al. A real-time game theoretic planner for autonomous two-player drone racing. *arXiv preprint arXiv:1801.02302*, 2018.